Relationship between Electrical Behavior and Structural Characteristics in Sr-Doped $LaNi_{0.6}Fe_{0.4}O_{3-\delta}$ Mixed Oxides

T. Montini,[†,‡] M. Bevilacqua,[†,‡] E. Fonda,[§] M. F. Casula,[||] S. Lee,[⊥] C. Tavagnacco,[†] R. J. Gorte,[⊥] and P. Fornasiero*[,†,‡]

Chemistry Department and INSTM-Trieste, University of Trieste, via L. Giorgieri 1, I-34127 Trieste, Italy, ICCOM-CNR Trieste Research Unit, Centre of Excellence for Nanostructured Materials, via L. Giorgieri 1, I-34127 Trieste, Italy, Synchrotron SOLEIL L'Orme des Merisiers, St. Aubin-BP48, 91192 Gif sur Yvette Cedex, France, Chemistry Department and INSTM-Cagliari, University of Cagliari, Monserrato, I-09042 Cagliari, Italy, and Department of Chemical and Biomolecular Engineering, University of Pennsylvania, 311A Towne Building, 220 South 33rd Street, Philadelphia, Pennsylvania 19104

Received February 16, 2009

A series of $La_{1-x}Sr_xNi_{0.6}Fe_{0.4}O_3$ mixed oxides were synthesized by a coprecipitation method, followed by calcination at 1000 °C. Materials with $x < 0.100$ exhibited a rhombohedral structure similar to that observed for $La_{0.4}Ni_{0.6}Fe_{0.4}O_3$, whereas materials with x between 0.125 and 0.150 were orthorhombic. The unit-cell volume decreased linearly from $x = 0$ to $x = 0.090$, but increased for increasing Sr^{2+} content. Materials with still higher Sr content (x between 0.200 and 0.300) exhibited additional XRD reflections indicating the limit of Sr solubility into to the perovskite. The electrical conductivity of the $La_{1-x}Sr_xNi_{0.6}Fe_{0.4}O_3$ increased continuously up to $x = 0.090$, but decreased sharply when the Sr^{2+} content was increased to $x = 0.100$ or higher. However, no such discontinuity was observed in the ionic conductivities. The specific electrical behavior of these materials is discussed on the basis of equilibrium between two possible charge-compensation mechanisms. The first mechanism pictures La^{3+} substituted by Sr^{2+} in the A site of the perovskite, resulting in the oxidation of the cations hosted in the B site of the structure (Ni and/or Fe). The second charge-compensation mechanism implies the formation of one oxygen vacancy for every two Sr^{2+} ions.

Introduction

Perovskites with ABO_3 structure can be prepared with a large variety of A (lanthanides, Ca^{2+}, Sr^{2+}, Ba^{2+}) and B (Mn, Fe, Ni, Co, Cu, Ga, Al, Mg, etc.) cations. These materials show interesting electrical conductivity properties for prospective application in solid oxide fuel cell (SOFC) cathodes[1−6] and electrolytes,[4,7−11] ceramic membrane reactors,[12−15] and catalysts,[16−21] mainly because of the possibility to combine electronic and ionic conductivity. An appropriate selection of the A and B cations can result in materials with very good mixed conductivity. For example, in the case of ferrites (B = Fe), the electronic and oxygen-ionic conductivity of $LaFeO_3$ can be enhanced by doping the A site with Sr^{2+}: a moderate amount of dopant increases the concentration of mobile oxygen vacancies and p-type charge carriers, whereas a Sr^{2+} content above 50% results in vacancy clustering and hole localization processes, with a detrimental effect on the performance of the material.[22−24]

---

* Corresponding author. Tel.: 39 040 558 3973. Fax: 39 040 558 3903. E-mail: pfornasiero@units.it.

[†] University of Trieste.

[‡] Centre of Excellence for Nanostructured Materials.

[§] Synchrotron SOLEIL L'Orme des Merisiers.

[||] University of Cagliari.

[⊥] University of Pennsylvania.

(1) Mamak, M.; Metraux, G. S.; Petrov, S.; Coombs, N.; Ozin, G. A.; Green, M. A. *J. Am. Chem. Soc.* **2003**, *125*, 5161.
(2) Mai, A.; Haanappel, V. A. C.; Uhlenbruck, S.; Tietz, F.; Stover, D. *Solid State Ionics* **2005**, *176*, 1341.
(3) Petitjean, M.; Caboche, G.; Siebert, E.; Dessemond, L.; Dufour, L. C. *J. Eur. Ceram. Soc.* **2005**, *25*, 2651.
(4) Hsu, M. F.; Wu, L. J.; Wu, J. M.; Shiu, Y. H.; Lin, K. F. *Electrochem. Solid State* **2006**, *9*, A193−A195.
(5) Baumann, F. S.; Fleig, J.; Cristiani, G.; Stuhlhofer, B.; Habermeier, H. U.; Maier, J. *J. Electrochem. Soc.* **2007**, *154*, 931.
(6) Serra, J. M.; Buchkremer, H. P. *J. Power Sources* **2007**, *172*, 768.
(7) Asamoto, M.; Shirai, H.; Yamaura, H.; Yahiro, H. *J. Eur. Ceram. Soc.* **2007**, *27*, 4229.
(8) Su, X. T.; Yan, Q. Z.; Ma, X. H.; Zhang, W. F.; Ge, C. C. *Solid State Ionics* **2006**, *177*, 1041.
(9) Gauckler, L. J.; Beckel, D.; Buergler, B. E.; Jud, E.; Muecke, U. R.; Prestat, M.; Rupp, J. L. M.; Richter, J. *Chimia* **2004**, *58*, 837.
(10) Pena-Martinez, J.; Marrero-Lopez, D.; Ruiz-Morales, J. C.; Buergler, B. E.; Nunez, P.; Gauckler, L. J. *J. Power Sources* **2006**, *159*, 914.
(11) Shaula, A. L.; Yaremchenko, A. A.; Kharton, V. V.; Logvinovich, D. I.; Naumovich, E. N.; Kovalevsky, A. V.; Frade, J. R.; Marques, F. M. B. *J. Membr. Sci.* **2003**, *221*, 69.
(12) Zhu, X. F.; Wang, H. H.; Yang, W. S. *Chem. Commun.* **2004**, 1130.
(13) Kharton, V. V.; Yaremchenko, A. A.; Valente, A. A.; Sobyanin, V. A.; Belyaev, V. D.; Semin, G. L.; Veniaminov, S. A.; Tsipis, E. V.; Shaula, A. L.; Frade, J. R.; Rocha, J. *Solid State Ionics* **2005**, *176*, 781.
(14) Wang, H.; Tablet, C.; Schiestel, T.; Werth, S.; Caro, J. *Catal. Commun.* **2006**, *7*, 907.
(15) Caro, J.; Wang, H. H.; Tablet, C.; Kleinert, A.; Feldhoff, A.; Schiestel, T.; Kilgus, M.; Kolsch, P.; Werth, S. *Catal. Today* **2006**, *118*, 128.
(16) Alifanti, M.; Florea, M.; Somacescu, S.; Parvulescu, V. I. *Appl. Catal. B-Environ.* **2005**, *60*, 33.
(17) Isupova, L. A.; Sutormina, E. F.; Kulikovskaya, N. A.; Plyasova, L. M.; Rudina, N. A.; Ovsyannikova, I. A.; Zolotarskii, I. A.; Sadykov, V. A. *Catal. Today* **2005**, *105*, 429.
(18) Tien-Thao, N.; Alamdari, H.; Zahedi-Niaki, M. H.; Kaliaguine, S. *Appl. Catal., A* **2006**, *311*, 204.
(19) Singh, U. G.; Li, J.; Bennett, J. W.; Rappe, A. M.; Seshadri, R.; Scott, S. L. *J. Catal.* **2007**, *249*, 349.
(20) Lim, S.; Moon, D.; Kim, J.; Kim, Y.; Park, N.; Shin, J. *J. Nanosci. Nanotechnol.* **2007**, *7*, 4013.
(21) Natile, M. M.; Poletto, F.; Galenda, A.; Glisenti, A.; Montini, T.; De Rogatis, L.; Fornasiero, P. *Chem. Mater.* **2008**, *20*, 2314.

10.1021/cm900467c CCC: $40.75

The oxygen-ionic conductivity is often expressed as the diffusion of an oxide ion hopping from the site where it is hosted to an adjacent empty site. This means that a minimum concentration of oxygen vacancies must be present in the crystal structure to ensure good ionic conductivity.[25,26] This is the case for well-known electrolytes for SOFCs based on doped ZrO_2, where Y^{3+}, Sc^{3+}, and Ca^{2+} dopants have been widely investigated to increase the material conductivity.[27] Similarly, $La_{1-x}Sr_xGa_{1-y}Mg_yO_{3-\delta}$ (LSGM)[11,28] shows high ionic conductivity due to its disordered structure of oxygen vacancies.[29]

The electronic conductivity in oxides usually takes place by the "small polaron mechanism". A small polaron involves the trapping of an electron or hole at one site by the local lattice polarization which it causes.[30] An electron or hole corresponds to a change of oxidation state of one atom, and this will cause a change in the lengths of neighboring bonds and sometimes a more complicated alteration of coordination geometry. Under most common conditions, the small polarons must move from site to site by a thermally activated hopping process. It is reported that electron conduction takes place through the B−O−B electrical transport,[31−33] being highly influenced by the overlapping between the O 2p and the transition metal 3d orbitals.[34,35] The extent of the overlap strongly depends on the B−O distance and on the B−O−B angle[36] and, therefore, on the local symmetry around the B cations that is dominated by the crystal structure of the perovskite. In general, the higher the symmetry (in the order orthorhombic, rhombohedral, tetragonal, and cubic), the higher the electronic conductivity. For example, in the case of the Fe/Co-based perovskites, the electrical conductivity is lower when A cations with smaller ionic radii are used, as a result of the distortion of the BO6 octahedra induced by the void space around the A site.[31−33,37−39] Moreover, it is reasonable that the presence of oxygen vacancies results in a significant decrease in the electronic conductivity because of the lack of the B−O−B bridges required for electron diffusion.

Recently, $LaNi_{1-x}Fe_xO_3$ (LNF) has attracted attention as a potential cathode for IT-SOFC.[40−47] A study carried out in one of our laboratories show that $LaNi_{0.6}Fe_{0.4}O_3$ has excellent electrical conductivity and demonstrated a correlation between conduction properties and phase homogeneity and microstructure.[45] The synthetic conditions necessary for obtaining homogeneous materials with suitable porosity and high conductivity were optimized.[45] Here we extend our previous work on $LaNi_{0.6}Fe_{0.4}O_3$ by investigating the effect of Sr^{2+} doping on the A site of the perovskite (LSNF). To our knowledge, the doping with Sr^{2+} of LNF materials has received only limited attention.[47−50] For example, whereas the effect of Sr^{2+} introduction into LNF was studied by Chiba et al.,[48] this work focused on Fe-rich materials because only the Fe-rich samples were obtained as single-phase materials using their solid-state synthesis procedure. Zhu et al.[49] reported the potential use of $La_{0.4}Sr_{0.6}Ni_{0.2}Fe_{0.8}O_3$ as a cathode material for SOFC in combination with a samaria-doped ceria (SDC) electrolyte. Using Mössbauer spectroscopy, Tsipis et al.[50] demonstrated that doping with Sr^{2+} resulted in the formation of Fe^{4+} and Ni^{4+} in $La_{1-y}Sr_yFe_{1-x}Ni_xO_{3-\delta}$ ($x = 0-0.2$; $y = 0.1-0.2$) at low temperature; they also reported that the addition of Sr^{2+} caused a structural transition (from orthorhombic to rhombohedral) and the formation of oxygen vacancies at higher temperatures.

In our case, wet chemical synthesis allowed preparation of homogeneous materials for Ni-rich materials, enabling us to investigate compositions that have not been reported previously. The influence of Sr^{2+} concentration and phase homogeneity on the structure and on the electronic conductivity of the obtained materials will be discussed in relation to structural modifications and possible charge compensation mechanisms.

Experimental Section

Preparation of the Samples. $La_{1-x}Sr_xNi_{0.6}Fe_{0.4}O_3$ (LSNF) materials, with Sr molar percentages ranging from 0 to 30 mol %, were prepared by coprecipitation, as previously reported for the undoped material.[45] $La(NO_3)_3\cdot XH_2O$ (99.9% Aldrich, 38.10% La_2O_3), $Ni(NO_3)_2\cdot 6H_2O$ (puriss.Fluka), $Fe(NO_3)_3\cdot 9H_2O$ (puriss.

---

(22) Patrakeev, M. V.; Bahteeva, J. A.; Mitberg, E. B.; Leonidov, I. A.; Kozhevnikov, V. L.; Poeppelmeier, K. R. *J. Solid State Chem.* **2003**, *172*, 219.

(23) Diethelm, S.; Van herle, J.; Sfeir, J.; Buffat, P. *J. Eur. Ceram. Soc.* **2005**, *25*, 2191.

(24) Tsipis, E. V.; Patrakeev, M. V.; Kharton, V.; Yaremchenko, A. A.; Mather, G. C.; Shaula, A. L.; Leonidov, I. A.; Kozhevnikov, V. L.; Frade, J. R. *Solid State Sci.* **2005**, *7*, 355.

(25) West, A. R. *Solid State Chemistry and Its Applications*; John Wiley & Sons: New York, 1987.

(26) West, A. R. *Chem. Rec.* **2006**, *6*, 206.

(27) Wincewicz, K. C.; Cooper, J. S. *J. Power Sources* **2005**, *140*, 280.

(28) Ishihara, T.; Matsuda, H.; Takita, Y. *Solid State Ionics* **1995**, *79*, 147.

(29) Kajitani, M.; Matsuda, M.; Hoshikawa, A.; Oikawa, K. I.; Torii, S.; Kamiyama, T.; Izumi, F.; Miyake, M. *Chem. Mater.* **2003**, *15*, 3468.

(30) Cox, P. A., *Transition Metal Oxides*; Oxford Science Publications: Oxford, U.K., 1992.

(31) Tai, L. W.; Nasrallah, M. M.; Anderson, H. U.; Sparlin, D. M.; Sehlin, S. R. *Solid State Ionics* **1995**, *76*, 259.

(32) Tai, L. W.; Nasrallah, M. M.; Anderson, H. U.; Sparlin, D. M.; Sehlin, S. R. *Solid State Ionics* **1995**, *76*, 273.

(33) Dasgupta, N.; Krishnamoorthy, R.; Jacob, K. T. *Mater. Sci. Eng., B* **2002**, *90*, 278.

(34) Deng, Z. Q.; Zhang, G. G.; Liu, W.; Peng, D. K.; Chen, C. S. *Solid State Ionics* **2002**, *152*, 735.

(35) Uhlenbruck, S.; Tietz, F. *Mater. Sci. Eng., B* **2004**, *107*, 277.

(36) Torrance, J. B.; Lacorre, P.; Nazzal, A. I.; Ansaldo, E. J.; Niedermayer, C. *Phys. Rev. B* **1992**, *45*, 8209.

(37) Kostogloudis, G. C.; Ftikos, C. *Solid State Ionics* **1999**, *126*, 143.

(38) Riza, F.; Ftikos, C.; Tietz, F.; Fischer, W. *J. Eur. Ceram. Soc.* **2001**, *21*, 1769.

(39) Xu, Q.; Huang, D.; Chen, W.; Zhang, F.; Wang, B. *J. Alloys Compd.* **2007**, *429*, 34.

(40) Chiba, R.; Yoshimura, F.; Sakurai, Y. *Solid State Ionics* **1999**, *124*, 281.

(41) Chiba, R.; Yoshimura, F.; Sakurai, Y. US6120924, 2000.

(42) Orui, H.; Watanabe, K.; Chiba, R.; Arakawa, M. *J. Electrochem. Soc.* **2004**, *151*, A1412−A1417.

(43) Arai, H.; Chiba, R.; Komatsu, T.; Orui, H.; Sugita, S.; Tabata, Y.; Nozawa, K.; Watanabe, K.; Arakawa, M.; Sato, K. *J. Fuel Cell Sci. Technol.* **2008**, *5*, 0312041.

(44) Zhou, X. D.; Yang, J. B.; Thomsen, E. C.; Cai, Q.; Scarfino, B. J.; Nie, Z.; Coffey, G. W.; James, W. J.; Yelon, W. B.; Anderson, H. U.; Pederson, L. R. *J. Electrochem. Soc.* **2006**, 153.

(45) Bevilacqua, M.; Montini, T.; Tavagnacco, C.; Vicario, G.; Fornasiero, P.; Graziani, M. *Solid State Ionics* **2006**, *177*, 2957.

(46) Bevilacqua, M.; Montini, T.; Tavagnacco, C.; Fonda, E.; Fornasiero, P.; Graziani, M. *Chem. Mater.* **2007**, *19*, 5926.

(47) Konysheva, E.; Invine, J. T. S. *J. Power Sources* **2009**, in press.

(48) Chiba, R.; Yoshimura, F.; Sakurai, Y. *Solid State Ionics* **2002**, *152*, 575.

(49) Zhu, G.; Fang, X.; Xia, C.; Liu, X. *Ceram. Int.* **2005**, *31*, 115.

(50) Tsipis, E. V.; Kiselev, E. A.; Kolotygin, V. A.; Waerenborgh, J. C.; Cherepanov, V. A.; Kharton, V. V. *Solid State Ionics* **2008**, *179*, 2170.

Fluka), $Sr(NO_3)_2$ (≥99% Fluka) and tetramethyl ammonium hydroxide, TMAH (25% in H_2O, Aldrich), were used as starting materials. To avoid silicon contamination of the samples, we prepared all the solutions using plastic labware.

Briefly, stoichiometric amounts of La, Sr, Ni, and Fe nitrates were dissolved in water to obtain a 0.1 M solution (total moles of cations per L of solution). The cation solution was added dropwise to a 1.0 M water solution of TMAH under vigorous stirring. To ensure full precipitation of the mixed hydroxides, the amount of base was 4 times that required by the stoichiometry. A green-yellow precipitate was obtained, which was aged at room temperature for 1 h before being filtered with ash-free paper filter. The gelatinous precipitate was suspended in water (10 g L^{-1} with respect to the final mixed oxide) and stirred overnight to remove the excess of base. Afterward, the precipitate was filtered, dried at 120 °C for 24 h, ground in a mortar, and calcined at 700 °C for 5 h in a static oven. ICP-MS analyses of mother liquor from filtration confirmed complete precipitation of the cations.

Characterization. Before any characterization, the powders were calcined at higher temperature in order to densify the samples used for both electrical and ionic conductivity measurements. In a typical preparation, the powders were calcined in air at 1000 °C for 5 h with a heating rate of 3 °C min^{-1} and a cooling rate of 4.5 °C min^{-1}. Finally, the calcined samples were stored in air.

The dc electrical conductivities (σ) of the samples were measured in air in the temperature range between 200 and 700 °C, using a 4-probe method (silver wires 0.25 mm diameter 99.9% Aldrich; silver conductive ink Alfa Aesar) with an Amel model 5000 potentiostat-galvanostat and a HP3478A multimeter. Prior to the measurements, the samples were formed into bars (20 × 2 × 2 mm) by uniaxially pressing the powder that had been calcined at 1000 °C for 5 h.

Ionic conductivities measurements were carried out in a membrane reactor as previously described.[51] Briefly, powders with $x = 0$, 0.090, and 0.150 were pressed in the form of disks (diameter of 12 mm and a thickness between 3 and 3.6 mm), calcined at 1500 °C for 5 h, and then attached to the end of a YSZ tube. The oxygen permeating through each specimen was then measured by balancing the steady-state permeation flux to the rate of oxygen pumped electrochemically across two Pt electrodes placed on opposite sides of the YSZ tube. The permeation fluxes were measured with the outside of the membrane exposed to air, whereas the $P(O_2)$ on the inside was between 0.02 and 0.04 atm.

Powder XRD patterns were recorded on the ground powders calcined at 1000 °C for 5 h using a X3000 Seifert diffractometer equipped with a graphite monochromator on the diffracted beam. The scans were collected within the range of 5−90° (2°) using Cu Kα radiation. The XRD patterns were fit using the PowderCell 2.4 program to determine the cell parameters and the homogeneity of the materials.

BET surface areas of the samples were measured by Kr physisorption at liquid nitrogen temperature (−196 °C) on the bars previously degassed at 350 °C for 12 h, using a Micromeritics ASAP 2020 apparatus.

Morphological images of the bars were recorded using a Leica Stereoscan 430i scanning electron microscope (SEM).

Transmission electron microscopy (TEM) analysis was performed using a JEOL 200CX TEM equipped with a tungsten cathode operating at 200 kV on the finely ground samples (previously calcined at 1000 °C for 5 h) deposited on a carbon-coated copper grid. TEM bright-field (BF) and dark-field (DF) images and selected-area electron diffraction (SAED) patterns were collected in order to investigate the structural features of the samples at different Sr loadings.

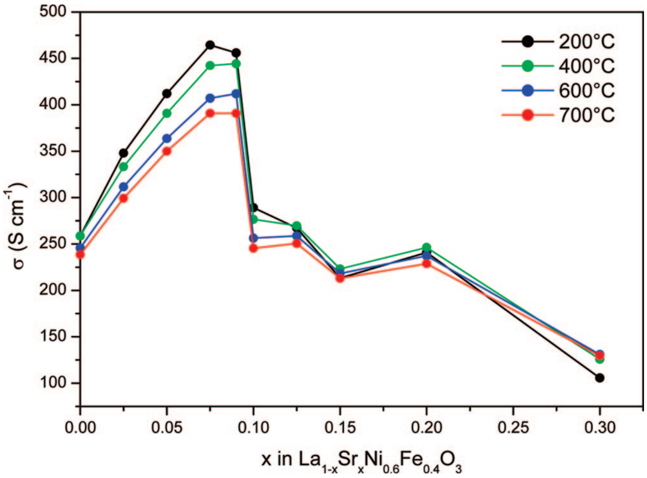

Figure 1. Effect of the Sr^{2+} amount on the electrical conductivity (σ) at different temperatures.

Thermogravimetric analyses (TGA) were performed on the LSNF samples with $x = 0$, 0.090, and 0.150 using a TA Instruments apparatus. Before the analysis, the powders were calcined at 1000 °C for 4 h in air. The changes in weight of the samples were measured while using a heating rate of 3 K/min under an air flow rate of 10 mL/min, up to a maximum temperature of 1000 °C.

EXAFS and XANES spectra have been recorded at the SAMBA beamline of SOLEIL synchrotron radiation center. Harmonic rejection was obtained by using two Pd-coated Si mirrors, whereas the Si (220) monochromator was operated fully tuned. Measurements were performed in the transmission mode at room temperature; beam intensity was measured before and after samples and reference foils by ionization chambers. EXAFS spectra were recorded at the K edges of Fe (7112 eV) and Ni (8333 eV). Samples were prepared by deposition on a PVDF membrane after grinding the powders, previously calcined at 1000 °C for 5 h, in an agate mortar, followed by ultrasonic suspension in isopropanol.

Data analysis has been performed with the Feffit code[52] using theoretical standards calculated with Feff 8.2[53] on the basis of model structures previously reported for LNF.[54] Data fitting in *r*-space was extended up to 0.4 nm and multiple scattering paths had to be included in the calculations; the most relevant were those involving the B−O−B paths that should carry information on the B−O−B angle.

Results and Discussion

Electrical Conductivity. The electrical conductivity (σ) for $La_{1-x}Sr_xNi_{0.6}Fe_{0.4}O_3$ materials measured at different temperatures is shown in Figure 1. For the LSNF materials, σ shows a continuous increment up to $x = 0.090$. A sharp and reproducible drop in the conductivity of the material is observed for Sr^{2+} content corresponding to $x = 0.100$. Notably, σ decreases to values similar to that of the undoped material. A further increase in the Sr^{2+} content leads to a further lowering of the conductivity, with a strong decrease for $x = 0.300$.

---

(51) Bidrawn, F.; Lee, S.; Vohs, J. M.; Gorte, R. J. *J. Electrochem. Soc.* **2008**, *155*, B660−B665.

(52) Newville, M. *J. Synchrotron Radiat.* **2001**, *8*, 322.

(53) Ankudinov, A. L.; Ravel, B.; Rehr, J. J.; Conradson, S. D. *Phys. Rev. B* **1998**, *58*, 7565.

(54) Falcon, H.; Goeta, A. E.; Punte, G.; Carbonio, R. E. *J. Solid State Chem.* **1997**, *133*, 379.

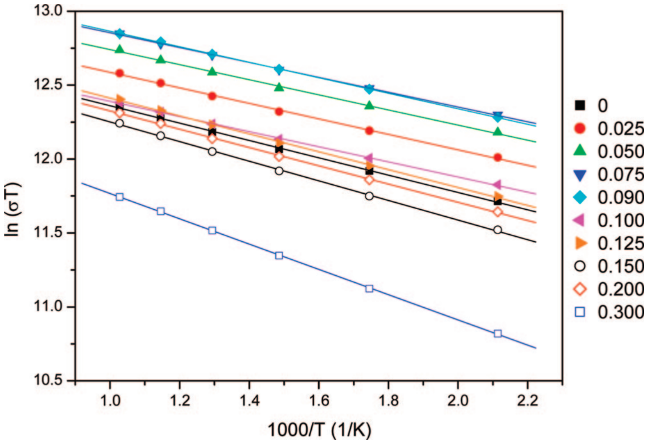

Figure 2. Arrhenius plot for the LSNF materials.

Table 1. Activation Energies (E_a) Calculated on the Basis of the Data Presented in Figure 2 for the Different LSNF Samples

sample (*x*)	E_a (kJ/mol)
0	4.88
0.025	4.35
0.050	4.25
0.075	4.18
0.090	4.35
0.100	4.15
0.125	5.03
0.150	5.52
0.200	5.14
0.300	7.10

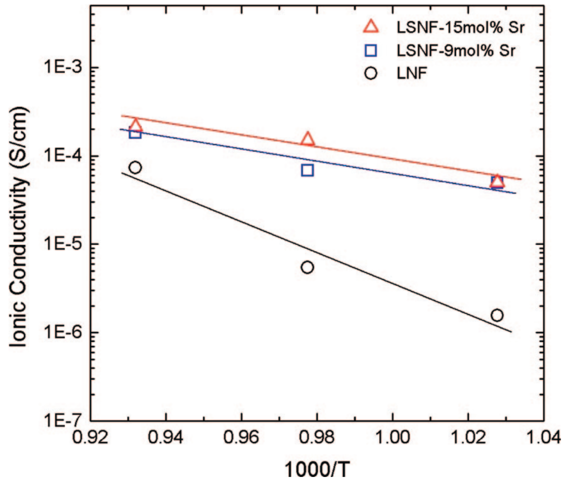

Figure 3. Ionic conductivity for the LSNF samples with $x = 0$, $x = 0.090$, and $x = 0.150$.

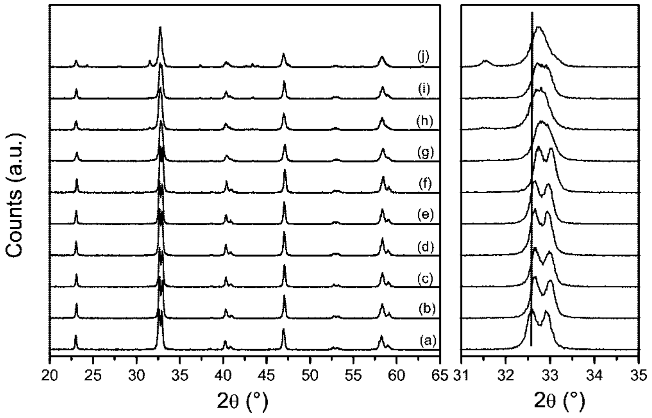

Figure 4. Powder XRD patterns recorded for the LSNF samples: (a) $x = 0$, (b) $x = 0.025$, (c) $x = 0.050$, (d) $x = 0.075$, (e) $x = 0.090$, (f) $x = 0.100$, (g) $x = 0.125$, (h) $x = 0.150$, (i) $x = 0.200$, and (j) $x = 0.300$. Part 1, overall view; part 2, detail of the main reflection.

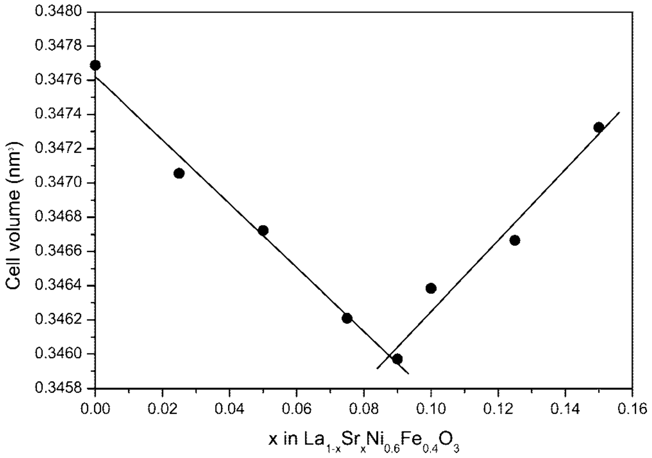

Figure 5. Variation in the cell volume of the major phase in the LSNF samples up to $x = 0.150$.

According to the small polaron conduction mechanism previously discussed for the undoped material,[45] the apparent activation energy (E_a) of the conductive process was calculated by the relationship between $\ln(\sigma T)$ and the reciprocal absolute temperature; straight lines were obtained with correlation coefficients $R^2 \geq 0.99$ as reported in Figure 2. The quality of the fit is an indication that the electric conductivity of the doped materials can be described by the small polaron mechanism, independently from the crystal structure and the homogeneity of the materials. The low values of E_a obtained for all the investigated samples (Table 1) suggest that the conductivity is essentially electronic. With respect to the undoped material, a slight decrease in the activation energy is observed up to $x = 0.10$, where E_a is approximately 4.2−4.3 kJ/mol. For higher Sr^{2+} contents, the activation energy increases, up to 7.1 kJ/mol for $x = 0.30$.

Ionic Conductivity. Ionic conductivities are believed to play a key role in limiting the performance of ceramic electrodes. The ionic conductivities of representative LSNF samples are shown as a function of temperature in Figure 3. It is worth noting that, as pointed out previously,[51] these experiments were carried out under conditions similar to that experienced by an SOFC cathode, i.e., the permeation fluxes were measured with $P(O_2)$ near 0.21 atm. Notably, the ionic conductivity of each of the samples was more than 1 order of magnitude lower than that of LSF ($La_{0.8}Sr_{0.2}FeO_3$),[51] which is a good mixed-conducting material. The introduction of Sr^{2+} leads to a significant increase in ionic conductivity over that of the undoped material but the ionic conductivity remains rather low. The difference between $x = 0.090$ and $x = 0.150$ is negligible; certainly there is no evidence for a maximum in the ionic conductivity corresponding to that in the electronic conductivity.

Structural and Morphological Characterization. The XRD patterns recorded for the LSNF samples calcined at 1000 °C for 5 h are presented in Figure 4. The splitting of the main reflection due to the tilting of the octahedra constituting the perovskite with respect to the *c* axis indicates

Table 2. Cell Parameters Resulting from the Rietveld Fit of the XRD Profiles of the LSFN Samples

sample (x)	a (nm)	c (nm)	V (nm^3)
0	0.55001	1.32714	0.34769
0.025	0.54969	1.32627	0.34705
0.050	0.54935	1.32664	0.34672
0.075	0.54894	1.32666	0.34621
0.090	0.54885	1.32618	0.34597
0.100	0.54896	1.32723	0.34638
0.125	0.54860	1.33004	0.34667
0.150	0.54890	1.33110	0.34732

Table 3. Results of the Fitting of the EXAFS Signals at the K Edges of Ni and Fe

	Fe K edge		Ni K edge		
sample (x)	C.N.[a]	R (nm)	C.N.[a]	R (nm)	% NiO
0	6	0.1941(7)	6	0.1947(6)	0(1)
0.050	6.5(8)	0.1969(6)	5.1(5)	0.1950(6)	2(1)
0.075	5.4(8)	0.1959(5)	5.9(5)	0.1939(6)	0(1)
0.090	6.4(8)	0.1941(5)	6.7(5)	0.1955(5)	0(1)
0.100	6.1(8)	0.1961(5)	5.1(7)	0.1941(4)	0(1)
0.125	6.9(7)	0.1962(4)	6.1(7)	0.1943(8)	1(1)
0.150	5.3(1)	0.197(2)	4.4(7)	0.195(1)	6(1)
0.200	6.2(8)	0.1962(8)	4.4(7)	0.195(1)	9(1)

[a] Coordination Number for the first neighbor shell of O ions around the metal considered.

that materials with $x < 0.100$ exist as a rhombohedral structure ($R\bar{3}c$ space group), the same as that of the undoped material.[45,54] The progressive shift of the reflections to higher diffraction angles is indicative of a significant reduction in the cell parameters with respect to the undoped material (see below). The samples with $x = 0.125$ and 0.150 present a symmetrical principal reflection, which suggests a lower tilting effect of the octahedra of the perovskite and/or a change in the crystal structure from rhombohedral to orthorhombic. Because the quality of the fits using the rhombohedral $R\bar{3}c$ or the orthorhombic $Pnma$ space groups is similar, it is not possible to discriminate between the two crystal structures. For the materials with higher Sr^{2+} content ($x =$ 0.200 and 0.300), new reflections are observed together with those corresponding to the perovskite phase. The secondary phases are more clearly discernible in the sample with $x =$ 0.300. In particular, a tetragonal phase of composition $(La,Sr)_2(Ni,Fe)O_{4\pm\delta}$ (with the K_2NiF_4 structure) can be clearly detected (reflection at $2\theta = 31.5°$) together with traces of NiO (reflection at $2\theta = 43.3°$). An expanded view of selected XRD patterns is presented in Figure S1 to underline this aspect (see the Supporting Information). These results suggest that the solubility of Sr into $LaNi_{0.6}Fe_{0.4}O_3$ is limited to 15% replacement of La.

Table 2 reports the cell parameters resulting from the Rietveld refinements of the XRD profiles using PowderCell 2.4 and assuming the rhombohedral space group. The trend of the cell volume as a function of the Sr^{2+} content for the materials that were homogeneous on the XRD scale (up to $x = 0.150$) is reported in Figure 5. The cell volume decreases linearly with Sr^{2+} content up to $x = 0.090$. For higher Sr^{2+} contents, an increase in the cell volume is observed.

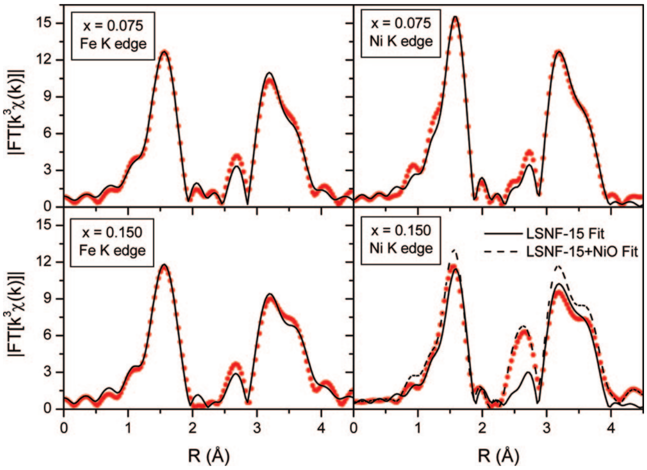

Figure 6. Real part of the FT of the EXAFS signal for LSNF samples with $x = 0.075$ and 0.150.

Table 3 summarizes the main structural results obtained by the analysis of the EXAFS signals recorded at the Fe and Ni K edge for the LSNF materials. Coordination numbers and distances are only shown for the first coordination shell, but distances and Debye−Waller factors for the shells up to 0.4 nm have been calculated to fit the data. Figure 6 shows representative results for the fitting of the EXAFS signals at both absorption edges for LSNF with $x = 0.075$ and 0.150. The analysis of the Fe K edge data provides evidence that ∼6 oxygen atoms are present in the first neighbor shell around the Fe ions, independent of the Sr^{2+} content. The EXAFS signals for both edges (Ni and Fe) experience a progressive modification due to the replacement of La with Sr and their different scattering factors witnessing an overall homogeneous doping of the structure. The detailed analysis of the Ni K edge shows that a coordination sphere composed of ∼6 oxygen ions is able to reconstruct with a good approximation the observed signal up to $x = 0.125$. For higher Sr^{2+} contents ($x = 0.150$ and 0.200), a component due to NiO must be taken into account in order to simulate the EXAFS signal correctly. By means of this example, Figure 6 shows the EXAFS signal of the Ni K edge for the sample with $x = 0.150$, which can be reasonably fit only by considering a linear combination of the signal deriving from a perovskite structure and that from NiO (which has an fcc-structure).The same result has been obtained introducing a supplementary contribution of a Ni−Ni distance at 0.296 nm. Other refinements with additional La or Sr contributions failed to fit the data. As for XRD, orthorhombic or rhombohedral structures are not so different to be easily distinguished and do not justify this additional feature. Although both the LSNF perovskite and NiO have a coordination number of 6 around Ni ions, the coordination number obtained from the EXAFS fitting is 4.5. This can be associated with a broad distribution of Ni−O distances. Therefore, a fit of the EXAFS experimental data using two Ni−O distances in the first shell was attempted. For the sample with $x = 0.150$, if the presence of 6% of NiO is assumed, two distances were found, 2.10 Å due to NiO and 1.94 Å belonging to LSNF. The resulting fit is able to nicely simulate the EXAFS signal and the refined total coordination number gets much closer to the expected value of 6. Similarly, the best simulation of the spectra of the sample with $x = 0.200$ was obtained assuming the presence of 9% of NiO.

Figure S2 (see the Supporting Information) reports the bright-field (BF) and corresponding dark-field (DF), along with SAED, obtained for the LSNF samples with a Sr^{2+} contents of $x = 0$ and $x = 0.150$. Both samples (as well as the other samples; data not reported) show polycrystalline grains, which give rise to the typical SAED pattern. The nanocrystalline domains can be imaged as bright areas in the DF image. From the TEM investigation, it was not possible to distinguish the presence of secondary phases such as NiO. No evident differences in morphology or crystal structure were observed among the samples.

TGA investigations were also used in order to identify changes in the stoichiometry of the LSFN materials as a function of temperature in air. In agreement with previous studies,[55] no significant weight changes were observed on representative samples of LSNF with $x = 0$, 0.090, and 0.150 for temperatures up to 1000 °C.

Kr physisorption measurements indicated that the surface areas of all samples ranged between 1.5 and 2.0 m^2/g with no appreciable correlation with the Sr^{2+} content. Similarly, the estimated porosity of the materials (calculated on the basis of the apparent and theoretical densities) was very similar for all the samples, showing no evident dependence on the Sr^{2+} doping level.

Representative SEM images of the materials prepared in form of bars are shown in Figure S3 (see the Supporting Information). In all the samples, grains with dimension around 0.2 μm and a narrow distribution are observed, as previously observed for the undoped material.[45] In agreement with the surface area measurements, a diffuse pore system is observed.

The morphological characterization of the LSNF materials highlights that the morphology of the materials is mainly determined by the preparation methodology rather than by the composition of the samples as previously reported in the case of the undoped material.[45] These results suggest that the peculiar conductivity properties observed for these materials (see above) are related mainly to the structural modifications induced by the introduction of Sr^{2+}, whereas the contribution of possible morphological charges (such as a different densification) is negligible.

Relationship between Structure and Conductivity. The following two charge compensating mechanisms could be involved when Sr^{2+} substitutes for La^{3+} in the crystal structure of the perovskite

$$SrO \xrightarrow{LSNF} Sr_{La}^{'} + Ni,Fe_{Ni,Fe} + O_O^x \qquad (1)$$

$$2\,SrO \xrightarrow{LSNF} 2\,Sr_{La}^{'} + V_O^{\bullet\bullet} + O_{2(g)} \qquad (2)$$

(eq 1) is related to the charge compensation mechanism in which the isomorphic substitution of La^{3+} with Sr^{2+} in the A site of the perovskite results in the oxidation of the cations hosted in the B site of the structure (Ni and/or Fe). These cations in the undoped materials are mainly in the (III) oxidation state.[46,54] (eq 2) is related to the charge compensation mechanisms in which the introduction of the aliovalent cation (Sr^{2+} instead of La^{3+}) results in the formation of one oxygen vacancy every two Sr^{2+} ions.

Notably, the charge compensation mechanisms have opposite effect on the cell volume. In fact, (eq 1) leads to a contraction of the cell parameters as a result of the lower ionic radius of the B cations, whereas the introduction of Sr^{2+} and the formation of the corresponding oxygen vacancies expressed in (eq 2) are both phenomena that reasonably slightly increase the cell lattice parameters because of the larger ionic radius of Sr^{2+} with respect to La^{3+} (0.144 and 0.132 nm respectively, for a XII coordination[56]). Therefore, the trend observed for the overall characteristics of the LSNF materials can be rationalized taking into account that both of the above mechanisms could be operative in the doped materials.

The oxidation in the B cations of the perovskite can be responsible for the linear decrease in the unit-cell volume with the Sr content up to $x = 0.090$. This hypothesis is corroborated by the linear decrease in the cell volume with the Sr^{2+} content, which perfectly fulfills the Vegard's law for an isostructural substitution of La^{3+} with Sr^{2+}. The cell volume decrease cannot be explained in terms of segregation of perovskites of different composition and/or oxides (NiO). In fact, because the ionic radius of Fe (III) (high-spin) is larger than that of Ni (III) (low-spin) (0.0645 and 0.056 nm, respectively, for a VI coordination [56]), a cell volume decrease can be observed only if the segregation of a Fe-rich compound would occur. Moreover, the substitution of La^{3+} with Sr^{2+} should result in an increase of the cell volume. Experimentally, the segregation of Ni-rich compounds is only observed for the materials with high Sr^{2+} contents, so it seems unlikely that there is segregation of Fe-rich compounds for the materials with low Sr^{2+} content. Consistently, the formation of electron holes as defects due to oxidation of the cations hosted in the B site of the perovskite (Ni and/or Fe) can justify the observed increase of the electronic conductivity. In fact, the presence of an electron hole on a B cation represents a favorable site where an electron can hope coming from a neutral B site. Moreover, the structural modifications induced by Sr^{2+} also contributes to reduce the distance between the two cationic positions (due to the reduction of the cell parameters) and/or the tilting of the oxygen octahedra around the B cations, allowing an increase of the overlapping of the atomic orbitals involved in the electron diffusion. Finally, the introduction of Sr^{2+} into the LNF structure also increase the ionic conductivity of the materials of about 1 order by magnitude with respect to the undoped material, as previously reported for other perovskites.[57-62] Although the charge compensation by B cations oxidation do not introduce oxygen vacancies into the

---

(55) Konysheva, E.; Irvine, J. T. S. *J. Mater. Chem.* **2008**, *18*, 5147.

(56) Shannon, R. D.; Prewitt, C. T. *Acta Crystallogr., Sect. B* **1969**, *25*, 925.

(57) Yasuda, I.; Ogasawara, K.; Hishinuma, M.; Kawada, T.; Dokiya, M. *Solid State Ionics* **1996**, *86*−*88*, 1197.

(58) Ullmann, H.; Trofimenko, N.; Tietz, F.; Stover, D.; Ahmad-Khanlou, A. *Solid State Ionics* **2000**, *138*, 79.

(59) Ullmann, H.; Trofimenko, N.; Naoumidis, A.; Stover, D. *J. Eur. Ceram. Soc.* **1999**, *19*, 791.

(60) Maguire, E.; Gharbage, B.; Marques, F. M. B.; Labrincha, J. A. *Solid State Ionics* **2000**, *127*, 329.

(61) Mineshige, A.; Izutsu, J.; Nakamura, M.; Nigaki, K.; Abe, J.; Kobune, M.; Fujii, S.; Yazawa, T. *Solid State Ionics* **2005**, *176*, 1145.

crystal structure, the observed increase in the ionic conductivity can be attributed to the formation of oxygen vacancies at high temperature, as previously reported for similar materials with Fe-rich composition[50] and for other good cathodic materials such as $(La,Sr)MnO_{3\pm\delta}$[63] and $(La, Sr)(Co, Fe)O_{3-\delta}$.[58,60–62]

The situation for the homogeneous LSNF materials with $0.090 < x < 0.150$ is different. The cell volume increase (Figure 5) is due to a combination of multiple effects. The formation of oxygen vacancies can explain the increase of the cell volume. In this range of Sr^{2+} concentrations, equilibrium between the two compensating mechanisms could be assumed: as the Sr^{2+} amount increases, this equilibrium moves to the formation of oxygen vacancies instead of the oxidation of the B cations. As a result, the cell volume increases because of the larger ionic radius of Sr^{2+} with respect to La^{3+} and to the lack of the cell constriction due to the shortening of the Ni/Fe−O length. However, the situation is complicated by the beginning of the decrease in the symmetry of the crystal structure and the change of the space group from rhombohedral to orthorhombic.

Segregation of phases with different composition and structure (such as NiO and $(La,Sr)_2(Ni,Fe)O_{4\pm\delta}$) is clearly observed by XRD only for $x > 0.200$, although EXAFS suggests the presence of trace amounts of NiO for $x = 0.150$ (see Table 3). A potential explanation is that the introduction of significant amounts of Sr^{2+}, with a larger ionic radius with respect to La^{3+}, could be incompatible with the rhombohedral structure determined by the large amount of Ni present in the B site. In this scenario, the segregation of Ni-rich compounds (tetragonal $(La,Sr)_2(Ni,Fe)O_{4\pm\delta}$ and NiO) could result in the enrichment of Fe in the B site and in the change of the structure from rhombohedral to orthorhombic. The last crystal structure is typical of LSNF material with Fe-rich compositions.[48−50] Because the ionic radius of Fe (III) (high spin) is larger than that of Ni (III) (low spin), the segregation of Ni could result in the increase of the unit-cell volume. A similar scenario has been recently reported by Striker et al.:[64] using synchrotron XRD measurements, the authors reported the presence of minor impurity phases in Sr-doped lanthanum ferrites, even when the samples appeared homogeneous using conventional XRD, accounted for lower electrical conductivities in the inhomogeneous materials.

For intermediate Sr^{2+} content ($x = 0.100−0.150$), oxygen vacancies could be introduced into the LSNF structure. It was previously reported that the presence of oxygen vacancies in perovskite materials reduces the electronic conductivity of the system.[65,66] Moreover, tetragonal $(La,Sr)_2(Ni,Fe)O_{4\pm\delta}$ phase present an electrical conductivity lower than that measured for our homogeneous LSNF materials.[67] As a result, the electronic conductivity should decrease and the activation energy increase because of the missing oxygen bridges between the cations.

Finally, in the case of the clearly inhomogeneous material ($x = 0.200$ and 0.300), a lower conductivity and a higher activation energy are observed because of the presence of crystal phases with low electric conductivity probably concentrated at the grain boundary.

Conclusions

A successful coprecipitation route for the preparation of LSNF perovskites in a wide compositional range allowed us to gain insights on the structure-conductivity relationship of $La_{1-x}Sr_xNi_{0.6}Fe_{0.4}O_3$ materials. The results, which are relevant for the design of cathodes for IT-SOFC, can be summarized as follows:

1. Homogeneous rhombohedral structure and low surface area $La_{1-x}Sr_xNi_{0.6}Fe_{0.4}O_3$ mixed oxides can be obtained by coprecipitation method followed by calcination at 1000 °C for $x \leq 0.150$.
2. The electrical conductivity of the $La_{1-x}Sr_xNi_{0.6}Fe_{0.4}O_3$ mixed oxides goes through a maximum at $x = 0.090$, the same composition at which the lattice parameter goes through a sharp minimum. We associate the decreasing electrical conductivity and increasing lattice parameter with the occurrence of oxygen-vacancy formation, possibly due to oxidation of some Ni and/or Fe.
3. XRD analysis suggests a lower tilting of the octahedra of the perovskite and/or a change in the crystal structure from rhombohedral to orthorhombic for $0.125 < x < 0.150$. For $x > 0.200$, the a tetragonal phase of composition $(La,Sr)_2(Ni,Fe)O_{4\pm\delta}$ is formed together with traces of NiO.

Acknowledgment. Prof. Mauro Graziani and Dr. G. Balducci (University of Trieste) are acknowledged for useful discussions. Dr. M. Cargnello (University of Trieste) is acknowledged for the technical assistance in the EXAFS measurements. We acknowledge SOLEIL for provision of synchrotron radiation facilities and we thank the staff for assistance in using the SAMBA beamline. The EXAFS experiments were supported by the European Community−Research Infrastructure Action under the FP6 “Structuring the European Research Area” Programme (through the Integrated Infrastructure Initiative “Integrating Activity on Synchrotron and Free Electron Laser Science”). University of Trieste, ICCOM-CNR, INSTM, FISR2002 “Nanosistemi inorganici ed ibridi per lo sviluppo e l’innovazione di celle a combustibile” are gratefully acknowledged for financial support. S.L. and R.J.G. acknowledge funding from the U.S. Department of Energy’s Hydrogen Fuel Initiative (Grant DE-FG02-05ER15721).

Supporting Information Available: Enlargement of XRD measurements, TEM images, and SEM for selected samples (PDF). This material is available free of charge via the Internet at http://pubs.acs.org.

CM900467C

---

(62) Wierczek, K.; Gozu, M. *J. Power Sources* **2007**, *173*, 695.

(63) Yasuda, I.; Hishinuma, M. *J. Solid State Chem.* **1996**, *123*, 382.

(64) Striker, T.; Ruud, J. A.; Gao, Y.; Heward, W. J.; Steinbruchel, C. *Solid State Ionics* **2007**, *178*, 1326.

(65) Gayathri, N.; Raychaudhuri, A. K.; Xu, X. Q.; Peng, J. L.; Greene, R. L. *J. Phys.: Condens. Mater.* **1998**, *10*, 1323.

(66) Bucher, E.; Sitte, W. *Solid State Ionics* **2004**, *173*, 23.

(67) Kharton, V. V.; Tsipis, E. V.; Naumovich, E. N.; Thursfield, A.; Patrakeev, M. V.; Kolotygin, V. A.; Waerenborgh, J. C.; Metcalfe, I. S. *J. Solid State Chem.* **2008**, *181*, 1425.